Journal of Ceramic Processing Research. Vol. 17, No. 6, pp. 523~531 (2016)

J O U R N A L O F
Ceramic Processing Research

Decoration of Ag nanoparticles on reduced graphene oxide and their application to gas sensors

Han Gil Na[a], Yong Jung Kwon[a], Sung Yong Kang[a], Wooseung Kang[b], Myung Sik Choi[a], Jae Hoon Bang[a], Taek Kyun Jung[c], Chongmu Lee[c] and Hyoun Woo Kim[a,d,*]

[a]*Division of Materials Science and Engineering, Hanyang University, Seoul 133-791, Korea*
[b]*Department of Metallurgical & Materials Engineering, Inha Technical College, Incheon 402-752, Korea*
[c]*Department of Materials Science and Engineering, Inha University, Incheon 402-791, Korea*
[d]*The Research Institute of Industrial Science, Hanyang University, Seoul 133-791, Korea*

We fabricated functionalized RGO that demonstrates excellent sensitivity to H_2S gas. The functionalization process used GO suspensions mixed with $AgNO_3$, NaOH, and DI water. X-ray diffraction (XRD) and transmission electron microscopy indicated that the functionalizing structures were composed of cubic Ag and silver oxide (Ag_xO_y) phases. Nanoparticles and nanorods with a cubic Ag phase were attached to the surface of the RGO. Raman spectra revealed that the structural disorder of the functionalized RGO was higher than that of pristine GO. The decrease of resistance by the introduction of H_2S gas indicated that the functionalized RGO was an n-type sensor. Accordingly, we suggested that the n-type Ag_xO_y, whose presence was confirmed by XRD, should be a main current path for the sensor. A H_2S gas sensing test revealed that the sensor response at 50 ppm was about 1.65. With respect to H_2S sensing mechanisms, we propose that the following four reasons could explain the significant enhanced sensitivity by the functionalization: (i) reduction of the conduction volume by the conduction through the Ag_xO_y structure rather than RGO, (ii) generation of silver sulfide structures, (iii) generation of an n-Ag_xO_y/p-RGO heterointerface, and (iv) larger surface area of Ag/Ag_xO_y structures. The Ag catalyst is not only the source of the Ag_xO_y, but also provides the spillover effect.

Key words: Ag, Reduced graphene oxide, Sensors.

Introduction

A variety of nanostructures has attracted enormous attention, as a result of their novel properties [1-25]. In recent years, graphene has attracted enormous interest in a variety of areas, including chemical gas sensing [26-29]. It has the lowest noise available and a very low detection limit, due to its high electron mobility [30]. Reduced graphene oxide (RGO) can be efficiently produced on a large scale by reducing graphene oxide (GO). RGO is effectively graphene functionalized by oxygen-containing species such as O, -OH, and -OOH groups; therefore, RGO has been regarded as a promising practical sensor [30].

In comparison to GO with its extremely low conductance, RGO can have a sufficiently high conductivity to guarantee its use as a conductance-based sensor. Also, compared with pure graphene, RGO has a considerable number of oxygen functional groups or other types of defects. These groups or defects provide the sites for superior adsorption of incoming gas molecules, contributing to sensitivity enhancement.

However, up to the present, the practical problems which realize the highly sensitive RGO or graphene have not been solved. By the way, the catalytic effect of Ag on sensitivity to various gases has been intensively studied. Ag has been used to enhance the sensitivity of various materials, such as Fe_2O_3 nanoparticles [31], carbon nanotubes (CNTs) [32], glass carbon electrodes [33], Ag@SnO_2 core-shell materials [34], Ag/SnO_2 composite nanotubes [35], WO_3 powders [36], Ag/ZnO nanocomposites [37], ZnO nanoflowers [38], and TiO_2 films [39]. Ag plays a catalytic role not only in the form of Ag doping [31, 36, 38], but also by modifying or decorating with Ag nanoparticles [32, 33, 35, 37] or thin films [39]. Depending on the sensing materials, Ag plays a catalytic role in sensing a variety of gases, including H_2 [39], phenyl hydrazine [38], CH_3CH_2OH, CH_3COCH_3, O_3 [37], NO [36], H_2O_2 [34,35], NO_2 [32], and NH_3 [32].

Accordingly, we suggest that the incorporation of Ag catalysts will pave the way to realization of RGO sensor. In this work, we have prepared composite materials from RGO and Ag nanostructures, comparing the characteristics of functionalized RGO, pristine RGO, and GO with respect to structure, morphology, and Raman properties. As a sensing gas, we have chosen H_2S gas, which is toxic and flammable. Exposure to a high concentration of H_2S, can cause immediate fainting and even death. In addition, extended exposure to a low concentration of H_2S gas results in eye irritation, sore throat, nausea, headache,

*Corresponding author:
Tel : +82-10-8428-0883
Fax: +82-2-2220-0299
E-mail: hyounwoo@hanyang.ac.kr

and dizziness. Accordingly, the detection of H_2S gas is extremely important. In spite of inherent low sensitivity of pristine RGO, the decoration of Ag resulted in a significant increase in gas sensitivity. We discussed the reason for the sensor enhancement.

Experimental

Our source materials were graphite powder, H_2SO_4 (98%), H_3PO_4 (98%), $KMnO_4$ (98%), H_2O_2 (30 wt%), hydrazine monohydrate (98%), DMF (99.8%) and

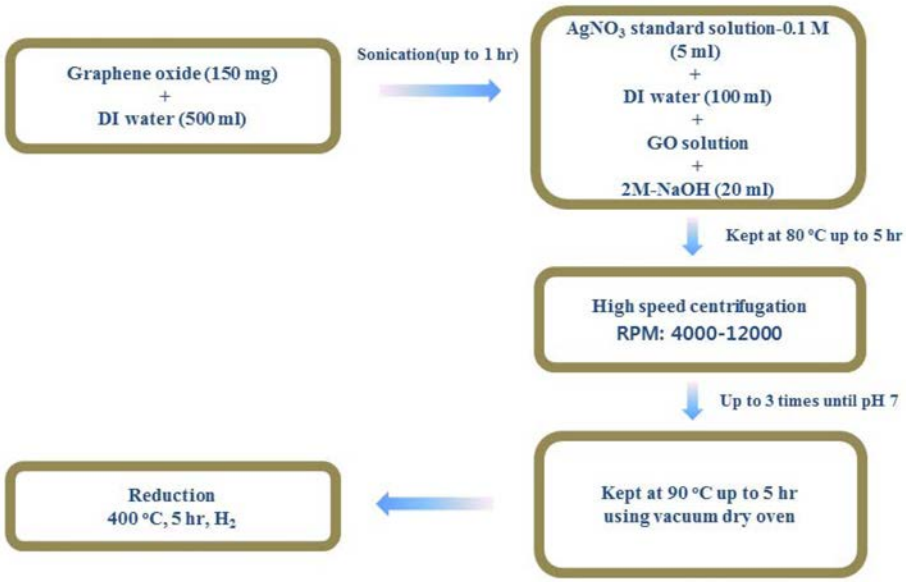

Fig. 1. Summary of experimental processes for the preparation of Ag-functionalized RGO.

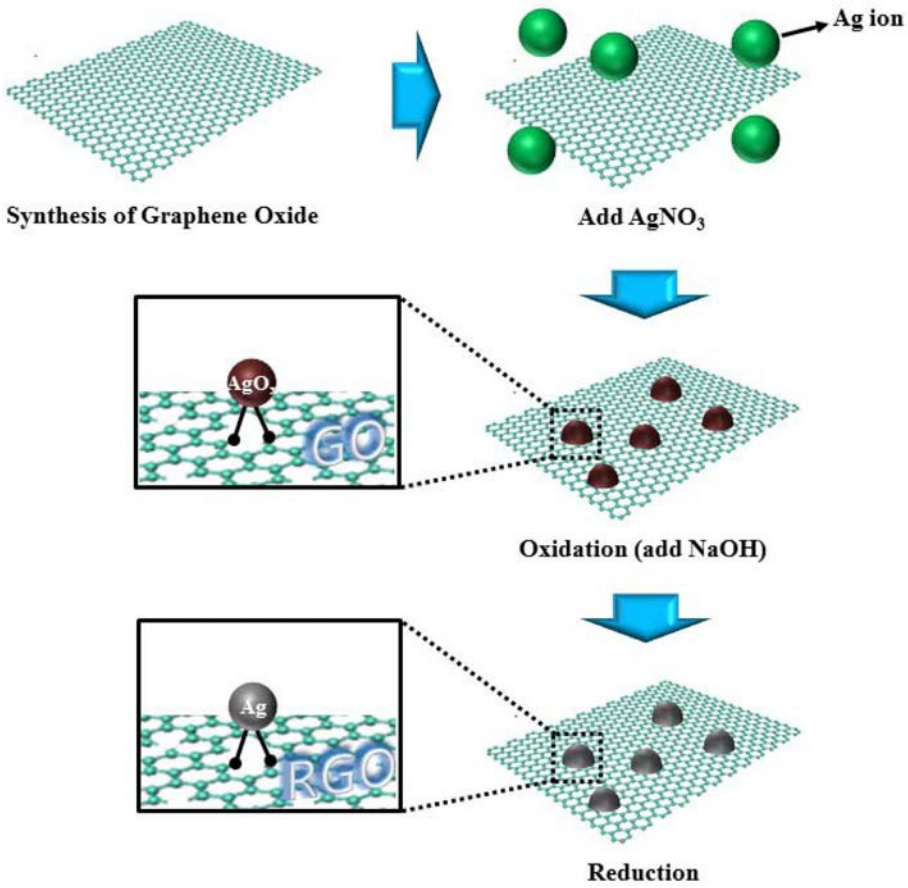

Fig. 2. Schematic outline of the experimental processes for the fabrication of Ag-functionalized RGO.

boric acid (H_3BO_3). GO was synthesized from graphite powder using a modification of Hummers and Offeman's method [40]. The experimental processes for the preparation of functionalized RGO composite materials are listed in Fig. 1 and schematically depicted in Fig. 2. The GO suspension consisted of GO powders (150 mg) and DI water (500 ml). After the GO suspension was sonicated for 1 h, it was mixed with 0.1 M $AgNO_3$ (50 ml), 2 M NaOH (20 ml), and DI water (100 ml). The solution was kept at 80 °C for 5 h. Following this, by the low-speed centrifugation at 4000 rpm, we removed thick multilayer sheets (i.e. all visible particles) for 15-20 min. Then the supernatant was further centrifuged at 8000-12000 rpm for 45 min, creating the solid GO-silver oxide (Ag_xO_y) nanoparticle composites. The high-speed centrifugation at 8000-12000 rpm was done several times until the solid composites reached the pH of 7. To remove all the moisture, the products were maintained in vacuum dry oven at 90 °C for 5 h. The annealing reaction was performed at 400 °C for 5 h in ambient ($Ar + H_2$) in a horizontal tube furnace. Finally, the system was cooled down to room temperature at a constant ($Ar + H_2$) flow rate of 120 sccm.

The samples were investigated using X-ray diffraction (XRD; *D/MAX Rint 2000* diffractometer model, Rigaku, Tokyo, Japan, CuKα radiation), field-emission scanning electron microscopy (FESEM, JSM-6700, JEOL Ltd., Tokyo, Japan), and transmission electron microscopy (TEM; a JEOL JEM-2010 transmission electron microscope, JEOL Ltd., Tokyo, Japan, 200 kV). Raman spectra were measured at room temperature by means of using a Jasco Laser Raman Spectrophotometer NRS-3000 Series at the Korean Basic Science Institute (KBSI). The power density and excitation laser wavelength were 2.9 $mW \cdot cm^{-2}$ and 532 nm, respectively.

In sensing experiments, we obtained films by spraying the as-prepared RGO-Ag suspension onto quartz substrates, which were located on a hot-plate at about 120 °C. Next, the products were kept in a vacuum dry oven at 90 °C for 5 h. By means of using an interdigital electrode mask, Ni/Au double-layer electrodes were sequentially sputtered onto the specimens. The base pressure of the sensor-residing vacuum chamber was kept at ~ 5×10^{-2} Torr. Previously, a similar experimental setup was reported [41-44]. At 250 °C, the sensor response was determined via the following formula: $S = R_a/R_{H2S}$, where R_a and R_{H2S} are the resistance of air and H_2S gas, respectively. The response and recovery times were calculated by the time taken to reach a 90% change in the resistance upon the supply or removal of the target gas, respectively [45].

Results and Discussion

Figs. 3(a), 3(b), and 3(c) show the XRD patterns of the GO, as-synthesized RGO, and Ag-functionalized RGO, respectively. In Fig. 3(b), we observe a strong and sharp (002) RGO diffraction line at 2è=25.60°. In Fig. 3(c), (111), (200), (220), (311), and (222) diffraction lines clearly show a cubic silver (Ag) phase with a lattice constant of a = 4.0855 Å (JCPDS card: No. 89-3722). We also identified a (11) line of monoclinic AgO with lattice constants of a = 5.852 Å, b = 3.478 Å, and c = 5. 495 Å (JCPDS card: No. 89-3081). Furthermore, the (100) line of the hexagonal Ag_2O phase is visible with lattice constants of a = 3.072 Å and c = 4.941 Å (JCPDS card: No. 72-2108). By the way, this peak also coincides with the (031) line of the monoclinic Ag_3O_4 phase with lattice constants of a = 3.5787 Å, b = 9.2079 Å, and c = 5. 6771 Å (JCPDS card: No. 40-1054).

Figs. 4(a)-4(c) show SEM images of as-synthesized RGO, and Figs. 4(d)-4(f) show those of Ag-functionalized RGO. One-dimensional rod-like structures and particle-like structures both appear on the RGO surface. The SEM and TEM investigations both revealed that particle-like and rod-like structures were deposited on the RGO surfaces. Figs. 5 and 6 indicate the results of TEM investigations with respect to rod-like and particle-like

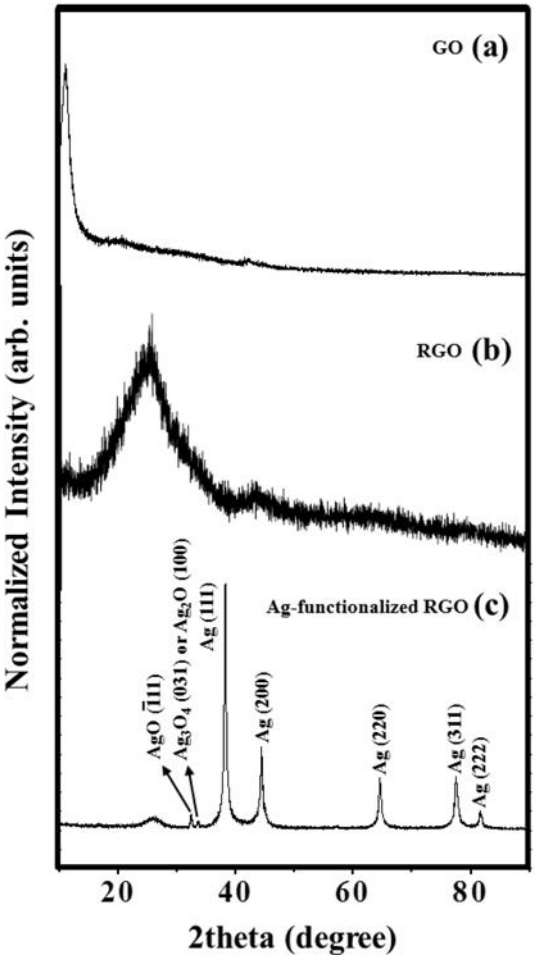

Fig. 3. XRD patterns of (a) GO, (b) as-synthesized RGO, and (c) Ag-functionalized RGO.

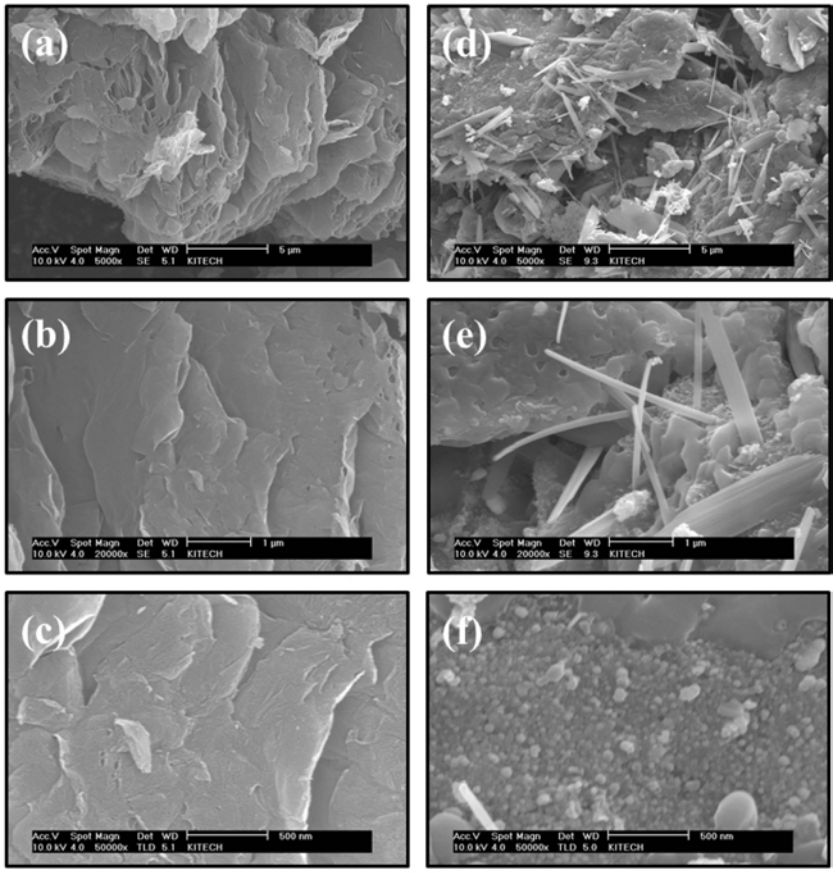

Fig. 4. SEM images of (a-c) as-synthesized RGO and (d-f) Ag-functionalized RGO.

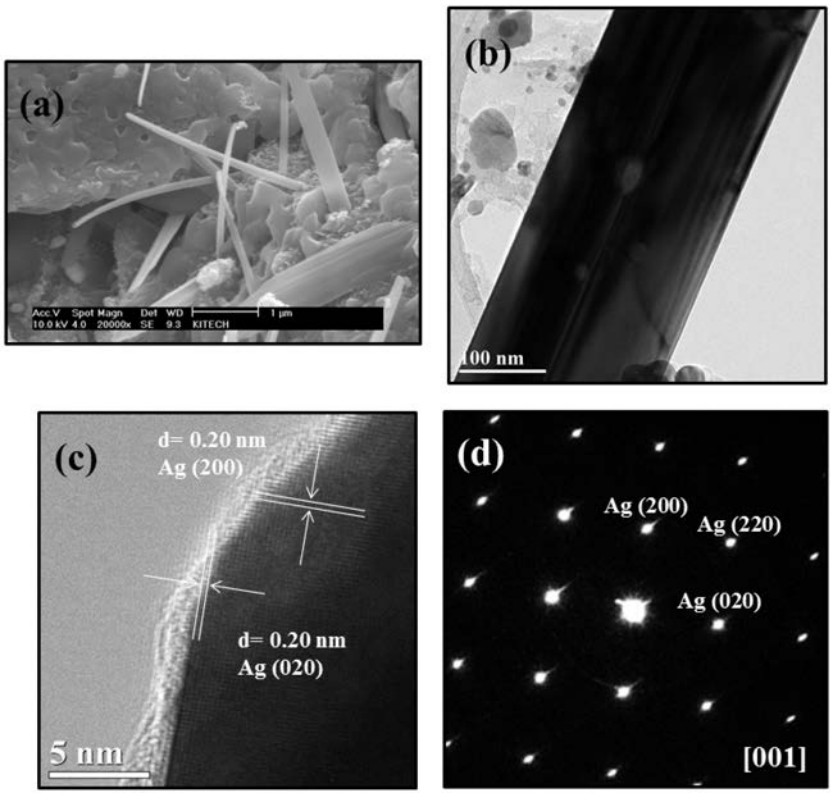

Fig. 5. (a) Typical SEM image and (b) TEM image of rod-like structures on RGO surfaces. (c) Lattice-resolved TEM image enlarging the surface region of a rod-like structure in (b). (d) Corresponding SAED pattern.

structures, respectively. Fig. 5(a) shows a SEM image of rod-like structures, and Fig. 5(b) shows a TEM image of a rod-like structure. Fig. 5(c) shows the lattice-resolved TEM image enlarging the surface region of the rod in Fig. 5(b). The spacing of the lattice fringes are about 0.20 nm, corresponding to the {200} lattice planes of cubic Ag. Fig. 5(d) shows the associated SAED pattern, clearly exhibiting diffraction spots of cubic Ag. Therefore, the rod-like structures are single-crystalline with the cubic Ag phase.

On the other hand, Fig. 6(a) shows a considerable number of particle-like structures on the RGO surface. Fig. 6(b) is a SEM image showing the deposition of particles on the RGO surface. Fig. 6(c) is a lattice-resolved TEM image for a particle in Fig. 6(b). The distances between neighboring fringes were measured to be 0.20 and 0.24 nm, close to those of the (200) and (111) lattice spacing in a primitive cubic Ag lattice. Fig. 6(d) is an associated SAED pattern, which reveals the existence of diffraction rings corresponding to the (111), (200), (220), and (311) planes of the cubic Ag phase. The existence of diffraction rings indicates that the particle-like structures are poly-crystalline.

Figs. 7(a), 7(b), and 7(c) exhibit the Raman spectra of the as-synthesized GO, as-synthesized RGO, and Ag-functionalized RGO. From our preliminary results, the precursor graphite showed the in-phase vibration of the graphite lattice (G band) at 1582 cm^{1} as well as the (weak) disorder band caused by the graphite edges (D

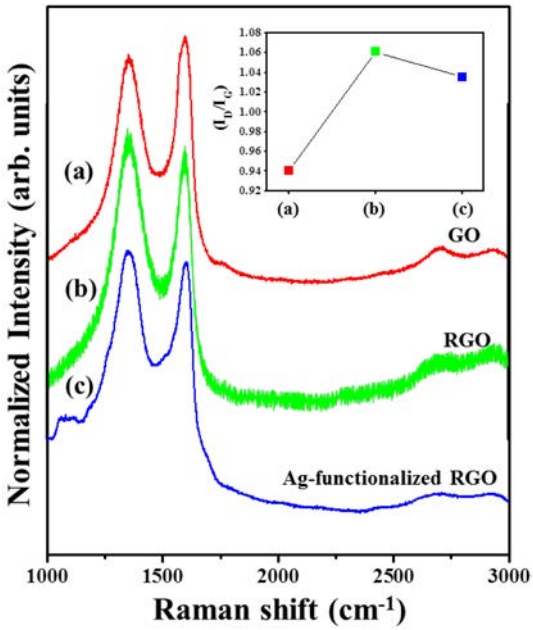

Fig. 7. Raman spectra of (a) as-synthesized GO, (a) as-synthesized RGO, and (c) Ag-functionalized RGO.

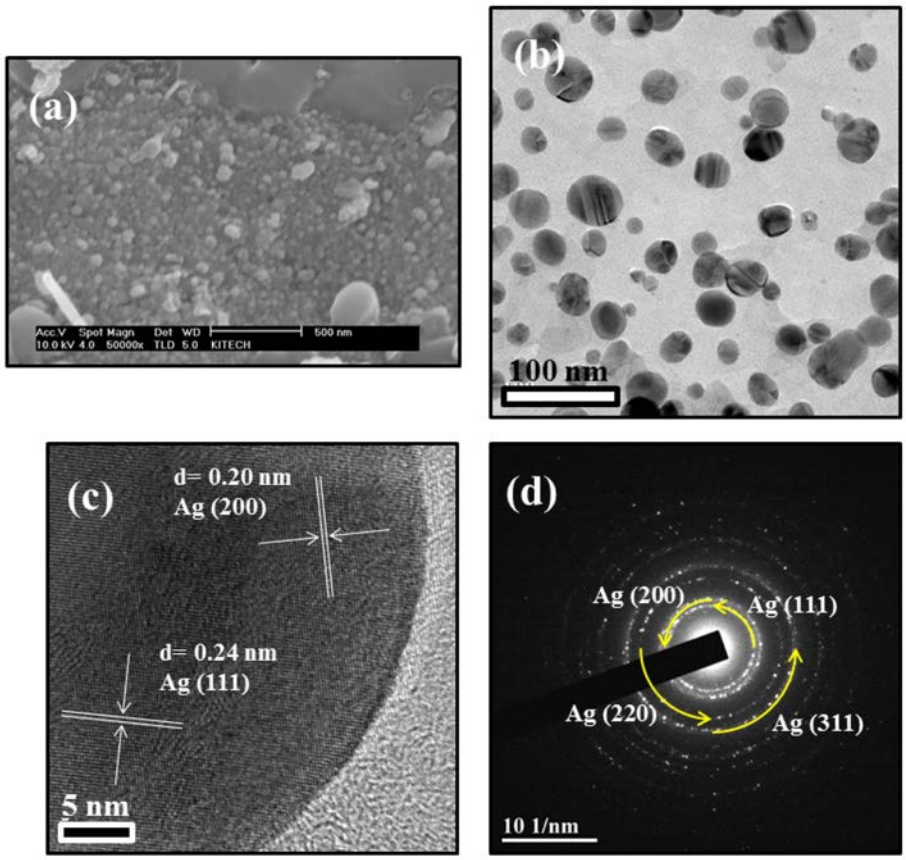

Fig. 6. (a) Typical SEM image and (b) TEM image of particle-like structures on RGO surfaces. (c) Lattice-resolved TEM image enlarging the surface region of a particle-like structure in (b). (d) Corresponding SAED pattern.

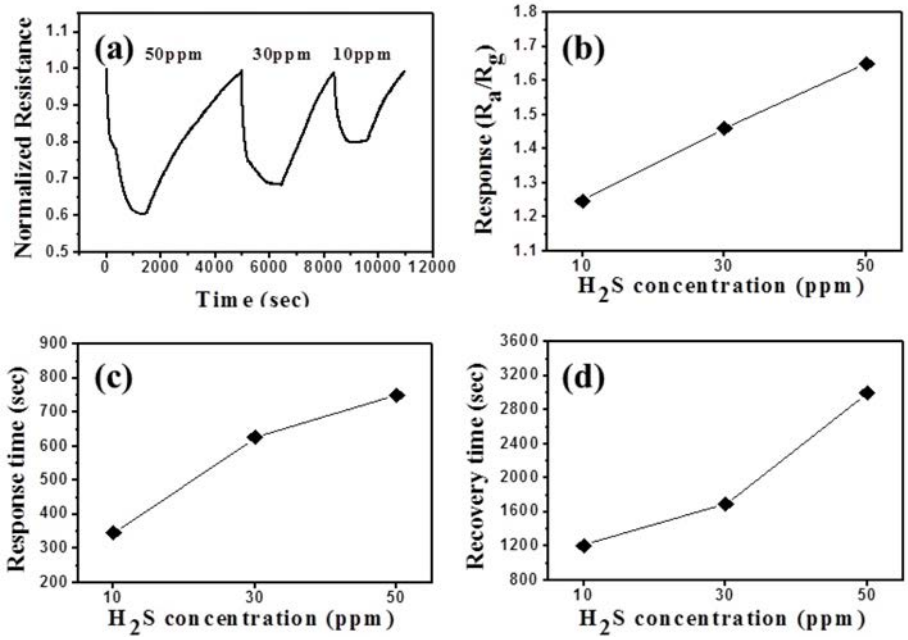

Fig. 8. (a) Dynamic response curves at H_2S concentrations of 10, 30, and 50 ppm, for the sensors fabricated from Ag-functionalized RGO. (b) Variation of sensor response with changing the H_2S concentration in the range of 10-50 ppm. (c) Response times for the sensors fabricated from as-synthesized RGO at the H_2S concentrations of 10, 30, and 50 ppm. (d) Recovery times for the sensors fabricated from as-synthesized RGO at the H_2S concentrations of 10, 30, and 50 ppm.

band) at approximately 1358 cm^1, with an intensity ratio of the D and G bands ($I_{(D)}/I_{(G)}$) of about 0.10 [46]. Raman spectra indicate that the $I_{(D)}/I_{(G)}$ values of the as-synthesized GO, as-synthesized RGO, and Ag-functionalized RGO are 0.9400, 1.0609, and 1.0353, respectively. Because an increase of the $I_{(D)}/I_{(G)}$ value represents an increase in the disorder of the structure, RGO is more disordered than GO. Furthermore, comparing the $I_{(D)}/I_{(G)}$ value of Ag-functionalized RGO to that of pristine GO reveals that a significant number of defects was generated in the preparation process. However, the $I_{(D)}/I_{(G)}$ value of Ag-functionalized RGO is slightly lower than that of the pristine RGO. Although the functionalization process includes a thermal annealing step, which may induce disorder in the RGO and contribute to the increase in the $I_{(D)}/I_{(G)}$ value, we surmise that the Ag nanoparticles and nanorods cover the defects on the RGO, contributing to the decrease in the $I_{(D)}/I_{(G)}$ value.

Fig. 8(a) shows the dynamic response curves for the sensors fabricated from the Ag-functionalized RGO. The concentration of H_2S gas was set to 10, 30, and 50 ppm. The resistance decreased and increased upon introducing and removing the H_2S gas, respectively, exhibiting n-type behavior. From the resistance values, we estimated that the sensor responses of the Ag-functionalized RGO at H_2S concentrations of 10, 30, and 50 ppm are about 1.25, 1.46, and 1.65, respectively.

The sensitivity will be defined as the following formula: $S = (R_a\text{-}R_{H2S})/R_{H2S}$, by which the sensitivity of the Ag-functionalized RGO at H_2S concentrations of 10, 30, and 50 ppm are about 0.25, 0.46, and 0.65,

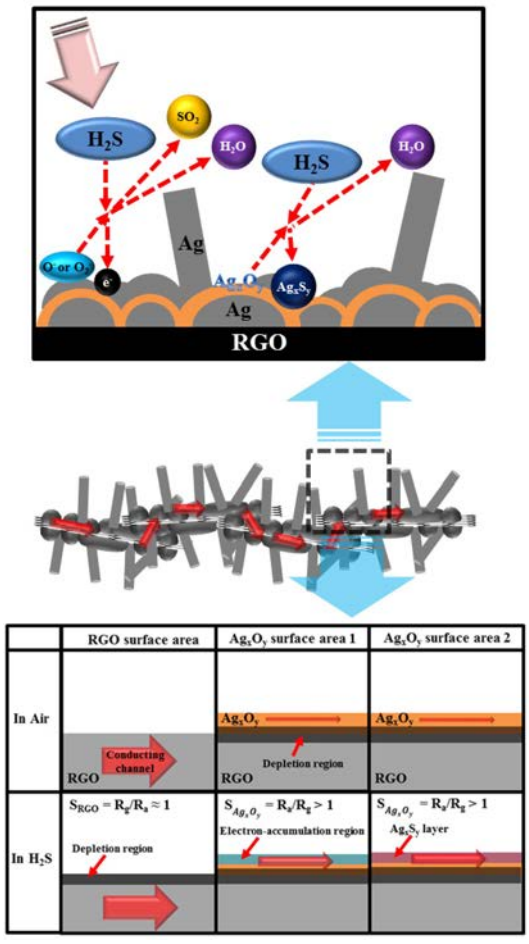

Fig. 9. Schematics explaining the sensing mechanisms of Ag-functionalized RGO in regard to H_2S gas.

respectively. It has been reported that the sensitivity of the RGO or graphene is relatively low, for example, 0.0017 for CO_2 [47], 0.0025 [48]-0.443 [49] for NO_2, 0.00251 for NO [50], 0.0071 for NH_3 [51], and 5.88 x 10^{-6} for SO_2 [50], etc. Also, it has been reported that Pd-decorated graphene exhibited a sensitivity of 0.04 for NO gas [52]. Accordingly, we reveal that the As-functionalization in the present work is very efficient in enhancing the sensitivity of the RGO sensor.

The response times of the Ag-functionalized RGO at H_2S concentrations of 10, 30, and 50 ppm are 346, 626, and 751 s, respectively. It has been reported that the response time of the RGO or graphene is 5 min for NO_2 [48], few min for SO_2 [50], etc. Also, it has been reported that Pd-decorated graphene exhibited a response time of 4 min for NO gas [52]. We think that the response time in the present functionalized RGO sensor is close to those of the previous literatures. The recovery times of the Ag-functionalized RGO at H_2S concentrations of 10, 30, and 50 ppm are 1211, 1691, and 2997 s, respectively. It takes longer for the whole sensing species to adsorb onto and desorb from the surface at higher concentrations.

Fig. 9 schematically depicts the H_2S sensing mechanisms of functionalized RGOs. Because the resistance decreased with the introduction of H_2S gas, the carrier concentration should increase. Pristine RGO possesses p-type semiconductor characteristics [53,54]. H_2S gas molecules react with the adsorbed oxygen species on the surface of the sensing materials. Assuming that O^- is usually regarded as the major oxygen adsorption species, the following H_2S sensing reaction should be considered [55,56];

$$H_2S(g) + 3O_{ad}^- \rightarrow SO_2(g) + H_2O(g) + 3e^-$$
$$2H_2S(g) + 3O_{ad}^- \rightarrow 2SO_2(g) + 2H_2O(g) + 3e^-$$

Accordingly, the introduction of H_2S gas donates electrons to the sensing materials. In this case, the hole concentration of RGO will decrease, decreasing the hole conductivity; this cannot contribute to the resistance decrease caused by the gas introduction in the present work. Therefore, conduction through the p-type RGO surface cannot explain the occurrence of n-type sensing behavior in the present study. Although most particles and rods are mainly composed of cubic Ag phase, as revealed by TEM investigation, it is possible that thin film-like silver oxide structures are deposited on the RGO surface. XRD investigation reveals that the functionalized RGO is composed of cubic Ag, monoclinic AgO, and hexagonal Ag_2O (or monoclinic Ag_3O_4) phases. We surmise that the silver oxide in the present work can be considered an n-type semiconductor. By the way, it is known that both AgO and Ag_2O are able to become an n-type semiconductor, if appropriately synthesized [57, 58]. On the other hand, to our knowledge, there has been no report on the n-type behavior of Ag_3O_4. Accordingly, it is more likely that the weak peak in Fig. 3(c) is Ag_2O (100) peak, rather than Ag_3O_4 (031) one.

Fig. 9 represents our expectation that the Ag_xO_y should be connected because n-type Ag_xO_y needs to be the main path for electric conduction. Because the functionalized RGO behaved as an n-type semiconductor in the present sensing test, we surmise that the Ag_xO_y played a major role in the sensing mechanisms. In our preliminary experiments, the pristine RGO exhibited very weak sensing signals, without making a noticeable difference by the introduction of H_2S gas. Several explanations are possible for the drastic improvement of sensing ability by the Ag-functionalization. First, H_2S gas molecules will react with the adsorbed oxygen species on the Ag_xO_y surface. We surmise that the donation of electrons by the introduction of H_2S gas increases the electron concentration of the Ag_xO_y structure, resulting in reduced resistance [55, 56]. On the other hand, when normal air is introduced, the H_2S at the surface will be eliminated by the newly adsorbed air molecules and thereby desorbed from the surface, ultimately resulting in increased n-type resistivity. In case of pristine p-type RGO sensor, the sensor response can be defined as $S = R_{H2S}/R_a$, where R_{H2S} and R_a are resistances measured with and without H_2S gas, respectively. Since the conduction volume in RGO is relatively large, the hole depletion region generated by H_2S gas is very small compared to the whole RGO volume. Accordingly, the sensor response will be close to 1. Therefore, pristine RGO exhibits a relatively low sensitivity under the normal and conventional sensor scheme. On the other hand, in the present case of the electron conduction through the n-Ag_xO_y shell, the sensor response can be defined as $S = R_a/R_{H2S}$, where R_{H2S} and R_a are resistances measured with and without H_2S gas, respectively. However, in the present case of Ag-functionalized one, thin Ag_xO_y structures take up a smaller volume than the whole RGO. When the accumulation volume is generated by the introduction of H_2S gas with consuming the surface depletion region by air ambient, the electron conductance will be significantly increased. Accordingly, R_{H2S} is significantly smaller than R_a. Accordingly, changes in electron concentration caused by the introduction and removal of H_2S gas in the small Ag_xO_y volume generate a large sensor response or sensitivity.

Second, it is possible that silver oxide will be sulfurized by reacting with H_2S gas:

$$AgO(s) + H_2S(g) \rightarrow AgS(s) + H_2O(g)$$
$$Ag_3O_4(s) + 4H_2S(g) \rightarrow Ag_3S_4(s) + 4H_2O(g)$$

Similarly, In_2O_3 reacts with H_2S gas, producing a conductive In_2S_3 structure [59]. It is possible that AgS or Ag_3S_4 has a high conductance and high free-carrier density. Accordingly, the generation of silver sulfide would increase the electron density and considerably

decrease the resistivity of the sensor.

Third, it is possible that the generation of an n-Ag_xO_y/p-RGO heterointerface will produce a depletion region, simultaneously reducing the carrier concentrations on both sides. Accordingly, when the depleted volume is generated by the introduction of an n-Ag_xO_y/p-RGO heterointerface, thin Ag_xO_y structures take up a much smaller conduction volume. When the depleted volume is generated by the introduction of H_2S gas, the electron conductance will be significantly increased. Accordingly, R_{H2S} is significantly smaller than R_a, contributing to further increase of the sensitivity.

Fourth, the Ag/Ag_xO_y structures with nanoparticles, nanowires, and films have a larger surface area, facilitating molecular absorption, gas diffusion, and mass transport. Its appropriate pseudo-pore space provides a lot of active center and efficient electron pathways for gas sensors.

Next, we speculate the detailed role of Ag catalysts. First, the Ag nanoparticles play a role in adsorbing the H_2S molecules, with respect to the spillover effect. The H_2S molecules will be preferentially adsorbed on the Ag surface, subsequently H_2S molecules migrating from the Ag to the silver oxide sites. XRD and TEM analyses both indicate that the nanoparticles are mainly comprised of cubic Ag. Second, providing more Ag catalysts generates more AgO_x, contributing to the enhancement of n-type behavior. Because H_2S gas molecules preferentially adsorb onto thin AgO_x structures rather than the underlying RGO (Fig. 9), the present sample will mainly assume an n-type nature [60-69].

Conclusions

In summary, we have fabricated Ag-functionalized RGO that exhibits sensing behavior to H_2S gas. The functionalization process utilized GO suspensions mixed with $AgNO_3$, NaOH, and DI water. XRD investigation revealed that the product is composed of not only cubic Ag phase, but also monoclinic AgO and Ag_3O_4 phases. SEM images show that both rod-like and particle-like structures are deposited on the RGO surface. Lattice-resolved TEM images and SAED patterns indicate that the rods and particles correspond to the cubic Ag phase. Both pristine RGO and Ag-functionalized RGO exhibit a higher $I_{(D)}/I_{(G)}$ value on the Raman spectrum than as-synthesized GO, indicating that the reduction and functionalization processes increase the degree of disorder. The sensor responses of the Ag-functionalized RGO at H_2S concentrations of 10, 30, and 50 ppm are about 1.25, 1.46, and 1.65, respectively. From the resistance curves, we expect that the functionalized RGO sensor will be n-type overall. We speculated about possible reasons for drastic enhancement of the RGO sensitivity by the functionalization. First, since the Ag_xO_y has a relatively smaller conduction volume than RGO, the change of resistance upon introduction and removal of H_2S gas will become greater. Second, the generation of metallic silver sulfide could increase the electron density, decreasing the resistivity of the sensor. Third, the generation of an n-Ag_xO_y/p-RGO heterointerface would further reduce the conduction volume in Ag_xO_y. Fourth, the Ag/Ag_xO_y structures have a larger surface area, facilitating molecular absorption, gas diffusion, and mass transport. We suppose that the role of the Ag catalyst is not only the source of Ag_xO_y, but also provides the spillover effect.

Acknowledgments

This research was supported by Basic Science Research Program through the National Research Foundation of Korea (NRF) funded by the Ministry of Education (2016R1A6A1A03013422).

References

1. L. Han, L. Zheng, Z. Hu, S, Yin and Y. Zeng, Electron. Mater. Lett. 10 (2014) 1-4.
2. Sh. Valedbagi, J. Jalilian, S. M. Elahi, S. Majidi, A. Fathalian and V. Dalouji, Electron. Mater. Lett. 10 (2014) 5-11.
3. M. S. Kale, Y. R. Toda, M. P. Bhole and D. S. Bhavsar, Electron. Mater. Lett. 10 (2014) 21-25.
4. S. Chawl, M. Saroha and R. K. Kotnala, Electron. Mater. Lett. 10 (2014) 73-80.
5. M. Khajelakzay and E. Taheri-Nassaj, Electron. Mater. Lett. 10 (2014) 117-120.
6. J.-W. Park and H. Lee, Electron. Mater. Lett. 10 (2014) 235-239.
7. H. S. Kim, K.-S. Ahn and S. H. Kang, Electron. Mater. Lett. 10 (2014) 345-349.
8. H. Zhang, Z. Li, J. Qian, Q. Guan, X. Du, Y. Cui and J. Zhang, Electron. Mater. Lett. 10 (2014) 433-437.
9. P. Wang, Y. Ju and A. Hosoi, Electron. Mater. Lett. 10 (2014) 503-507.
10. D.-W. Kim and P.-R. Cha, Electron. Mater. Lett. 10 (2014) 525-528.
11. Y. A. K. Reddy, B. Ajitha, P. S. Reddy, M. S. P. Reddy and J.-H. Lee, Electron. Mater. Lett. 10 (2014) 907-913.
12. S. Kim, G. Nam and J.-Y. Leem, Electron. Mater. Lett. 10 (2014) 915-920.
13. S. B. Jambure, G. S. Gund, D. P. Dubal, S. S. Shinde and C. D. Lokhande, Electron. Mater. Lett. 10 (2014) 943-950.
14. H.-A. Choi, H. Jang, H. Hwang, M. Choi, D. Lim, S. E. Shim and S.-H. Baeck, Electron. Mater. Lett. 10 (2014) 957-962.
15. N. K. Singh, B. Choudhuri, A. Mondal, J. C. Dhar, T. Goswami, S. Saha and C. Ngangbam, Electron. Mater. Lett. 10 (2014) 975-980.
16. J. S. Maeng, D. J. Choi, K.-O. Ahn and Y.-H. Kim, Electron. Mater. Lett. 10 (2014) 1019-1025.
17. L. R. Shobin and S. Manivannan, Electron. Mater. Lett. 10 (2014) 1027-103.
18. M. Zhuang, A. Wei, J. Liu, Y. Zhao and Z. Yan, Electron. Mater. Lett. 10 (2014) 1075-1079.
19. S.-K. Kim, C. J. Raj and H.-J. Kim, Electron. Mater. Lett. 10 (2014) 1137-1142.
20. R. Yu, J.-H. Pee, H.-J. Kim and Y. J. Kim, Electron. Mater.

Lett. 10 (2014) 1159-1162.
21. Y.-S. Cho and Y.-D. Huh, Electron. Mater. Lett. 10 (2014) 1185-1189.
22. J. H. Son, Y. H. Song, B. J. Kim and J.-L. Lee, Electron. Mater. Lett. 10 (2014) 1171-1174.
23. A. Sarkar, K. Kanakamedala, N. N. Jagadish, A. Jordan, S, Das, N. Siraj, I. M. Warner and T. Daniels-Race, Electron. Mater. Lett. 10 (2014) 879-885.
24. Y. Noh and O. Song, Korean J. Met. Mater. 52 (2014) 61-65.
25. S. J. Yoo and W. J. Kim, Korean J. Met. Mater. 52 (2014) 561-572.
26. F. Schedin, A. K. Geim, S. V. Morozov, E. W. Hill, P. Blake, M. I. Katsnelson and K. S. Novoselov, Nature Mater. 6 (2007) 652-655.
27. J. D. Fowler, M. J. Allen, V. C. Tung, Y. Yang, R. B. Kaner and B. H. Weiller, ACS Nano 3 (2009) 301-306.
28. Y. D. Dan, Y. Lu, N. J. Kybert, Z. T. Luo and A. T. C. Johnson, Nano Letters 9 (2009) 1472-1475.
29. M. W. K. Nomani, R. Shishir, M. Qazi, D. Diwan, V. B. Shields, M. G. Spencer, G. S. Tompa, N. M. Sbrockey and G. Koley, Sens. Actuators B 150 (2010) 301-307.
30. N. Chen, X. Li, X. Wang, J. Yu, J. Wang, Z. Tang and S. A. Akbar, Sens. Actuators B 188 (2013) 902-908.
31. Y. Wang, Y. Wang, J. Cao, F. Kong, H. Xia, J. Zhang, B. Zhu, S. Wang and S. Wu, Sens. Actuators B 131 (2008) 183-189.
32. C. Cui, H. Pu, E. C. Mattson, G. Lu, S. Mao, M. Weinert, C. J. Hirschmugl, M. Gajdardziska-Josifovska and J. Chen, Nanoscale 4 (2012) 5887-5894.
33. K. Liao, P. Lao, Y. Li, Y. Nan, F. Song, G. Wang and M. Han, Sens. Actuators B 181 (2013) 125-129.
34. R. J. Wu, D. J. Lin, M. R. Yu, M. H. Chen and H. F. Lai, Sens. Actuators B 178 (2013) 185-191.
35. Y. E. Niao, S. He, Y. Zhong, Z. Yang, W. W. Tjiu and T. Liu, Electrochim. Acta 99 (2013) 117-123.
36. L. Chen and S. C. Tsang, Sens. Actuators B 89 (2003) 68-75.
37. Q. Simon, D. Barreca, A. Gasparotto, C. Maccato, E. Tondello, C. Sada, E. Comini, A. Devi and R. A. Fischer, Nanotechnology 23 (2012) 025502.
38. A. A. Ibrahim, G. N. Dar, S. A. Zaidi, A. Umar, M. Abaker, H. Bouzid and S. Baskoutas, Talanta 93 (2012) 257-263.
39. S. Rahbarpour and S. M. Hosseini-Golgoo, Sens. Actuators B 187 (2013) 262-266.
40. W. S. Hummers and R. E. Offeman, J. Am. Chem. Soc. 80 (1958) 1339.
41. H. W. Kim, S. H. Shim, J. W. Lee, J. Y. Park and S. S. Kim, Chem. Phys. Lett. 456 (2008) 193-197.
42. S. W. Choi, J. Y. Park and S. S. Kim, Nanotechnology 20 (2009) 465603.
43. J. Y. Park, S. W. Choi, J. W. Lee, C. Lee and S. S. Kim, J. Am. Ceram. Soc. 92 (2009) 2551-2554.
44. J. Y. Park, S. W. Choi and S. S. Kim, Nanoscale Res. Lett. 5 (2010) 353-359.
45. H. W. Kim, S. W. Choi, A. Katoch and S. S. Kim, Sens. Actuators B 177 (2013) 654-658.
46. N. Kudin, B. Ozbas, H. C. Schniepp, R. K. Prud'homme, I. A. Aksay and R. Car, Nano Lett. 8 (2008) 36-41.
47. H. J. Yoon, D. H. Jun, J. H. Yang, Z. Zhou, S. S. Yang and M. M. C. Cheng, Sens. Actuators B 157 (2011) 310-313.
48. M. W. K. Nomani, R. Shishir, M. Qazi, D. Diwan, V. B. Shields, M. G. Spencer, G. S. Tompa, N. M. Sbrockey and G. Koley, Sens. Actuators B 150 (2010) 301-307.
49. W. J. Yuan, A. R. Liu, L. Huang, C. Li and G. Q. Shi, Adv. Mater. 5 (2012) 766-771.
50. G. G. Chen, T. M. Paronyan and A. R. Harutyunyan, Appl. Phys. Lett. 101 (2012) 053119.
51. T. H. Han, Y. K. Huang, A. T. L. Tan, V. P. Dravid and J. X. Huang, J. Am. Chem. Soc. 133 (2011) 15264-15267.
52. W. W. Li, X. M. Geng, Y. F. Guo, J. Z. Rong, Y. P. Gong, L. Q. Wu, X. M. Zhang, P. Li, J. B. Xu, G. S. Cheng, M. T. Sun and L. W. Liu, ACS Nano 5 (2011) 6955-6961.
53. S. Deng, V. Tjoa, H. M. Fan, H. R. Tan, D. C. Sayle, M. Olivo, S. Mhaisalkar, J. Wei and C. H. Sow, J. Am. Chem. Soc. 134 (2012) 4905-4917.
54. J. D. Fowler, M. J. Allen, V. C. Tung, Y. Yang, R. B. Kaner and B. H. Weiller, ACS Nano 3 (2009) 301-306.
55. N. S. Ramgir, P. K. Sharma, N. Datta, M. Kaur, A. K. Debnath, D. K. Aswak and S.K. Gupta, Sens. Actuators B 186 (2013) 718-726.
56. J. W. Yoon, Y. J. Hong, Y. C. Kang and J. H. Lee, RSC Advances 4 (2014) 16067-16074.
57. Z. Jiang, S. Huang and B. Qian, Electrochim. Acta 39 (1994) 2465-2470.
58. R. S. Perkins, B. V. Tilak, B. E. Conway and H. A. Kozlowska, Electrochim. Acta 17 (1972) 1471-1489.
59. W. Zang, Y. Nie, D. Zhu, P. Deng, L. Xing and X. Xue, J. Phys. Chem. C 118 (2014) 9209-9216.
60. J. Liu, Z. Zhai, G. Jin, Y. Li, F. F. Monica and X. Liu, Electron. Mater. Lett. 11 (2015) 34-40.
61. E. S. Babu, S.-K. Hong, T. S. Vo, J.-R. Jeong and H. K. Cho, Electron. Mater. Lett. 11 (2015) 65-72.
62. T. Ali, K. S. Karimov, K. M. Akhmedov, K. Kabotov and A. Harooq, Electron. Mater. Lett. 11 (2015) 259-265.
63. F. Meriche, T. Touam, A. Chelouche, M. Dehimi, J. Solard, A. Fischer, A. Boudrioua and L.-H. Peng, Electron. Mater. Lett. 11 (2015) 862-870.
64. S. H. Yoon, K. H. Lee and S. J. Hong, Korean J. Met. Mater. 53 (2015) 123-132.
65. M. S. Kim, G. Nam, D. Kim, H. E. Kim, H. Kang, W. B. Lee, H. Choi, Y. Kim and J.-Y. Leem, Korean J. Met. Mater. 53 (2015) 139-144.
66. T.-H. Lee, J.-W. Ha, H. Ryu and E.-J. Lee, Korean J. Met. Mater. 53 (2015) 591-599.
67. H.-C. Chae, W.-S. Yong, J.-W. Hong, Korean J. Met. Mater. 53 (2015) 642-647.
68. I. Kim, Y. Kim, G. Nam and J.-Y. Leem, Korean J. Met. Mater. 53 (2015) 745-750.
69. S. J. Kim, K. Choi and S.-Y. Choi, Korean J. Met. Mater. 53 (2015) 890-903.